Semiconductor Physics, Quantum Electronics & Optoelectronics, 2023. V. 26, No 2. P. 165-172

Semiconductor physics

A method for fast calculating the electronic states in 2D quantum structures based on $A^{III}B^{V}$ nitrides

V.A. Slipokurov[1], P.P. Korniychuk[2], A.V. Zinovchuk[2]

[1]*V. Lashkaryov Institute of Semiconductor Physics, NAS of Ukraine, 41, prosp. Nauky, 03680 Kyiv, Ukraine*
[2]*Zhytomyr Ivan Franko State University, 40, Velyka Berdychivska str., 10008 Zhytomyr, Ukraine*
**Corresponding authors e-mail: vic31slk@ukr.net, zinovchuk.a@zu.edu.ua*

Abstract. The paper presents a method for fast calculating the electronic states in two-dimensional quantum structures based on $A^{III}B^{V}$ nitrides. The method is based on the representation of electronic states in the form of a linear combination of bulk wave functions of materials, from which quantum structures are made. The parameters and criteria for the selection of bulk wave functions that provides fast convergence of the numerical procedures for calculating the eigenvalues of the quantum Hamiltonian have been considered. The results of the calculations have been given both for one polar InGaN/GaN quantum well and for a system of several quantum wells. Being based on the full band structure of $A^{III}B^{V}$ nitrides with a wurtzite-type crystal lattice, the proposed approach takes into account the states far from the center of the Brillouin zone, while preserving the computational efficiency of traditional methods of envelope function in approximating the effective mass.

Keywords: $A^{III}B^{V}$ nitrides, two-dimensional quantum structures, electronic states.

https://doi.org/10.15407/spqeo26.02.165
PACS 81.07.St, 85.35.Be

Manuscript received 01.03.23; revised version received 16.03.23; accepted for publication 07.06.23; published online 26.06.23.

1. Introduction

InGaN/GaN quantum wells were long used in optoelectronic devices as generators of visible radiation, mainly blue and green ones. The generation of red radiation in these systems was not available for a long time as caused by the large defectivity of $In_xGa_{1-x}N$ layers for $x > 0.3$ when they are grown on typical GaN or sapphire substrates. To overcome this problem, scientific groups proposed several technological innovations, such as growing on pseudo-substrates [1–7] and using the buffer layers to compensate for mechanical strains during growth [8–15].

As a result, in recent years publications began to appear reporting the successful use of InGaN/GaN systems in LEDs with the wavelength 633 nm [16] and even 740 nm [17]. Generation of all three RGB main colors by using only nitrides opens new possibilities for micropixel display technologies. However, the quantum efficiency of InGaN/GaN LEDs in the green-red area of the visible spectrum is significantly lower as compared to blue LEDs. The reasons for this phenomenon cannot be explained only by defectiveness of the $In_xGa_{1-x}N$ layers with a high In content. The physical mechanisms responsible for the drop in efficiency of InGaN/GaN LEDs are hidden in features of recombination and transport of charge carriers, which are difficult to be detected in a direct targeted experiment. That is why numerous modeling can provide answers to questions that are not available in experimental studies. However, such modeling is not trivial for several reasons.

The first reason lies in the fundamental multiphysics of modeling, that is, the combination of an electrodynamic model with a quantum-mechanical one. The second reason is the need to use iterative algorithms of self-consistency of the electrodynamic and quantum-mechanical models, since the results obtained in one of the models are the initial conditions for another. Usually, for InGaN/GaN quantum wells, it is implemented by combining the diffusion-drift model with the method of envelope functions for solving the Schrödinger equation [18]. In the simplest case, the method of envelope functions leads to the calculation of the eigenvalues of quantum systems described by the Hamiltonian in the effective mass approximation or its $k \cdot p$ generalization [19, 20], where the wave function of the quantum state is decomposed in the basis of the Bloch functions of the center of the Brillouin zone (or G-point) of materials from which the quantum systems are made. This

© V. Lashkaryov Institute of Semiconductor Physics of the NAS of Ukraine 2023
© Publisher PH "Akademperiodyka" of the NAS of Ukraine 2023

approach is the most effective in terms of the speed of finding a self-consistent solution, but it can be questioned regarding the physical relevance of the obtained results. One possible, more physically reasonable replacement for the method of envelope function can be the empirical method of strong coupling. The strong coupling method is currently the most widely used method for modeling the electron transport in InGaN/GaN structures [21–24]. Naturally, the modeling process requires more computing power and delays calculations, especially when it is used to find a self-consistent solution.

In this paper, we propose to consider another alternative to the method of envelope functions, which is called the method of linear combination of bulk bands (LCBB) [25, 26]. In its original formulation, the method is based on the decomposition of the wave function of nanostructure in the full (not only the center of the Brillouin zone like to that in $k\cdot p$ approximation) basis of the Bloch functions of the materials from which the nanostructure is made.

The Bloch functions themselves of bulk materials are obtained using the empirical pseudopotential method. In [27], the LCBB approach was considered in detail for the general type of 2D and 1D nanostructures, and general recommendations were given for choosing the basis of Bloch functions for decomposition of the wave function for nanostructures. The use of this approach to study electronic states and transport in Si, Ge, and GaAs nanostructures was also reported [28]. The purpose of this work is to identify the possibilities of the LCBB approach regarding the physical relevance and effectiveness of its application especially to polar InGaN/GaN quantum wells.

2. Theoretical model

By analogy with the linear combination of atomic orbitals, which is used in the strong coupling method, LCBB uses the representation of the quantum wave function in the form of a linear combination of the eigenstates of the bulk materials, from which the nanostructure is prepared. In our case, these materials were binary nitrides with a wurtzite-type crystal lattice. We used the empirical pseudopotential method to obtain eigen electronic states in bulk nitrides. In this work, we took into account only the local component of atomic pseudopotentials, which depends on the value of wave vector (k) according to the parametric relation:

$$V(k)=\Omega\sum_{i=1}^{4}b_{1i}\exp\left(-b_{3i}\left(k-b_{2i}\right)^2\right), \tag{1}$$

where $\Omega=\Omega_0/4$ (volume of GaN or InN unit cell). The numerical values for the parameters $\{b_{11}, b_{21}, \ldots, b_{34}\}$, which define the form of the pseudopotentials for each atom in the inverse space, were optimized by us to achieve the greatest correspondence to the latest experimental data and first-principles calculations for binary nitrides with a wurtzite-type crystal lattice. These target data were energies at the points of high symmetry of the Brillouin zone, effective masses, band gaps at the InN/GaN interface. Multi-objective optimization was performed using a simplex-type algorithm [29]. This algorithm does not require numerical calculations of the gradients for the highly nonlinear optimization functional, which significantly speeds up the procedure for finding the global optimal value, effectively discarding local optima. During the optimization, we did not take into account spin-orbit interaction effects and deformation effects that make insignificant corrections to the structure of the valence bands of binary nitrides [30]. The resulting set of parameters is adduced in Table 1.

In what follows, we will consider the LCBB formalism for 2D quantum well-type nanostructures. In these systems, the periodicity of the potential of the crystal lattice is violated only in one direction. In the future, we will call this direction the z-direction. This violation can be described by the potential $U(z)$ that is the quantum confinement potential. As a rule, the function $U(z)$ is obtained by self-consistent solution of the equations of the electronic transport model.

Since the goal of this work was not to build a complete transport model, we used the empirical form of the quantum confinement potential, which reproduces the main features of InGaN/GaN quantum wells (band gaps at heterointerfaces, the presence of an electric polarization field). Under the above conditions, the one-electron Schrödinger equation for the wave function $\psi(\vec{r},z)$ of the quantum state has the form

$$H\psi(\vec{r},z)=\left[-\frac{\hbar^2}{2m_0}\nabla^2+U_0(\vec{r},z)+U(z)\right]\psi(\vec{r},z)=E\psi(\vec{r},z), \tag{2}$$

where H is the Hamiltonian of the quantum structure, E is the eigenvalue, and $U_0(\vec{r},z)$ is the periodic potential of the crystal lattice. According to the LCBB formalism,

Table 1. Optimized parameters of atomic pseudopotentials. Parameters b_{11}, b_{12}, b_{13}, b_{14} are given in Ry/(Å)^3.

	GaN		InN	
	Ga	N	In	N
b_{11}	–1.455816	–0.430305	–1.405991	0.294541
b_{21}	–0.272695	–0.241202	–0.234410	–0.343970
b_{31}	2.013207	3.669188	1.955968	2.286919
b_{12}	0.192748	–0.922755	0.219729	–0.848754
b_{22}	1.961085	0.762030	1.754019	0.581173
b_{32}	0.857372	0.983282	1.458801	0.674031
b_{13}	0.241016	0.170734	0.285917	0.144111
b_{23}	2.171686	1.506516	2.146941	1.047892
b_{33}	1.217690	0.867399	4.221378	0.920193
b_{14}	–0.003961	0.009662	0.156405	0.043072
b_{24}	3.010995	2.797614	3.377304	2.959492
b_{34}	11.04524	13.30637	11.47290	15.92229

the wave function ψ is represented as a superposition of Bloch functions $\left|n\left(\vec{k},k_z\right)\right\rangle$ of bulk materials:

$$\psi(\vec{r},z)=\sum_{n,\left(\vec{k},k_z\right)} A_{n,\left(\vec{k},k_z\right)}\left|n\left(\vec{k},k_z\right)\right\rangle, \quad (3)$$

where k_z is the component of wave vector in the direction of quantization, $\vec{k}=\left(k_x,k_y\right)$ – wave vector in the plane perpendicular to the direction of quantization. Substituting (3) into (2) and taking into account the representation of each Bloch function as a product of a periodic function and a plane wave $\left|n\left(\vec{k},k_z\right)\right\rangle = u_{n\left(\vec{k},k_z\right)}\exp\left(i\left(\vec{k}\cdot\vec{r}+k_z\cdot z\right)\right)$, the matrix elements of the Hamiltonian H in the basis of the Bloch functions takes the form

$$\left\langle n\left(\vec{k},k_z\right)\right|H\left|n'\left(\vec{k},k_z'\right)\right\rangle=\frac{2\pi}{L_z}\sum_{n',k_z'}E_{bulk}^{(n)}\left(\vec{k},k_z\right)\delta_{k_z,k_z'}\delta_{n,n'}+$$

$$+\sum_{G_z}U\left(k_z'+G_z-k_z\right)\left\langle u_{n\left(\vec{k},k_z-G_z\right)}\middle|u_{n'\left(\vec{k},k_z'\right)}\right\rangle, \quad (4)$$

where $E_{bulk}^{(n)}\left(\vec{k},k_z\right)$ is the eigenvalue of the energy corresponding to the Bloch function of the bulk material $\left|n\left(\vec{k},k_z\right)\right\rangle$, $U\left(k_z\right)$ – Fourier image of the quantum confinement potential, $\left\langle u_{n\left(\vec{k},k_z-G_z\right)}\middle|u_{n'\left(\vec{k},k_z'\right)}\right\rangle$ – integral of the overlap between the periodic parts of bulk Bloch functions, G_z – component of the vector of the inversed lattice inherent to the bulk material, L_z – length of the nanostructure or the periodicity length related to the periodic boundary conditions imposed on the Schrödinger equation. Summation in equation (4) takes place over all numbers n' of energy bands of bulk materials and components of wave vectors k_z' belonging to the corresponding region in the Brillouin zone of bulk materials. The vector $\vec{k}$ enters (4) as a parameter and must belong to the first 2D Brillouin zone. According to the definition, the first 2D Brillouin zone is considered to be a region in the inverse space, in which two vectors $\vec{k}$ and $\vec{k}'$ are arbitrary and satisfy the condition $\vec{k}\neq\vec{k}'+\vec{G}$ for inverse lattice vectors such that $\vec{G}=\left(\vec{g}\neq 0,G_z\right)$.

A simple analysis shows that in the case of nitrides with a wurtzite-type crystal lattice, the entire set for $\vec{G}$ is limited to the following six vectors: $\vec{G}_{1,2}=\pm 2\pi/a\,(1,0,0)$, $\vec{G}_{3,4}=\pm 2\pi/a\left(-1/2,\sqrt{3}/2,0\right)$, $\vec{G}_{5,6}=\pm\left(\vec{G}_1+\vec{G}_2\right)$, where a is the crystal lattice constant of the quantization plane. As can be seen, all the vectors have zero components in the z-direction. Therefore, it is obvious that the condition $\vec{k}\neq\vec{k}'+\vec{G}$ is fulfilled for all $\vec{k}$ belonging to the hexagon of the base of the Brillouin zone for bulk nitrides (Fig. 1). Diagonalization of the matrix (4) for each $\vec{k}$ of the 2D Brillouin zones gives a spectrum of

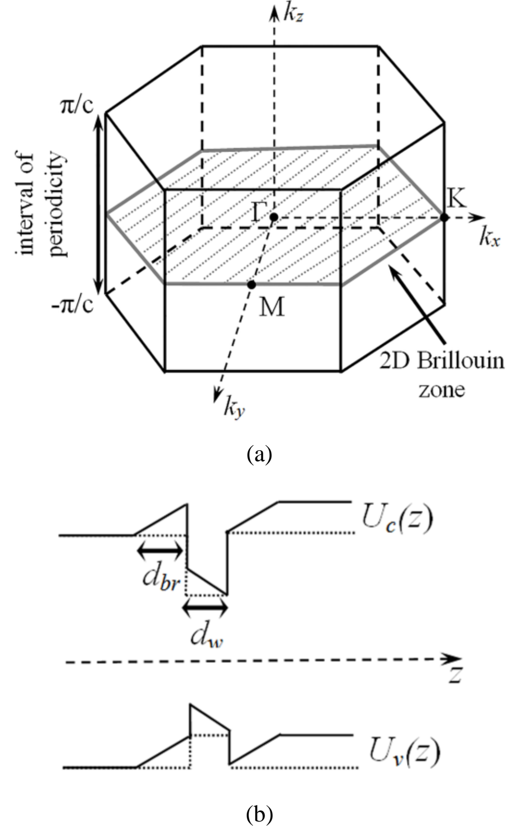

Fig. 1. a) 2D Brillouin zone and k_z interval of periodicity for polar InGaN/GaN quantum wells. b) Schematic view of quantum confinement potentials for electrons $U_e(z)$ and holes $U_h(z)$. Dashes show the form of potentials without account of the polarization effects in the well and barriers.

energy eigenvalues, which can be interpreted as an energy band diagram for 2D nanostructures. That is, vector $\vec{k}$ can be considered a kind of "quantum number" that "numbers" of quantum states in 2D structures.

As shown in [27], the set of k_z values, by which summation in (4) is actually carried out, must satisfy the condition $k_z\neq k_z'+G_z$ for all the components G_z that are included into the vectors of the inverse lattice $\vec{G}=\left(\vec{0},G_z\right)$. Again, taking into account the symmetry of the inverse space for a wurtzite-type crystal lattice, it can be ascertained that $G_z=\pm 2\pi/c$, where c is the crystal lattice parameter in the polar z-direction. Therefore, the condition $k_z\neq k_z'+G_z$ is fulfilled for all k_z from the interval $\left[-\pi/c;\,\pi/c\right]$. With account of this condition, formation of a linear combination of eigenstates of bulk materials was performed as follows. First, we choose $\vec{k}$ that belongs to the 2D Brillouin zone, and relate with it the system of vectors $\left(\vec{k},k_{z,i}\right)$, where the points $k_{z,i}=i\pi/N_{k_z}c$, $i\in\left[-N_{k_z};N_{k_z}\right]$ were uniformly placed within the interval $\left[-\pi/c;\,\pi/c\right]$. The number N_{k_z} will be referred to as the discretization number. For each

$\left(\vec{k}, k_{z,i}\right)$, we find eigenstates of bulk materials. Since formation of InGaN/GaN quantum well at the atomic level can be modeled using the random arrangement of In atoms in the GaN matrix, as the eigenenergy $E_{bulk}^{(n)}\left(\vec{k}, k_z\right)$ and Bloch functions $\left|n\left(\vec{k}, k_z\right)\right\rangle$, we used the corresponding values for GaN (*i.e.*, we used approximation of one bulk material).

Thus, the resulting Hamiltonian matrix (4) has the dimensionality $\left(2N_{k_z}+1\right)N_n$, where N_n is the number of bulk zones that were included in the calculation. As for summation over the components inherent to the vector of the inverse lattice G_z for the bulk material, which is present in (4), then, just as it was assumed in the work [27], we limited ourselves to only three terms with $G_z = 0, 2\pi/c, -2\pi/c$. Summation over the other G_z has almost no effect on the final result due to the rather rapid decrease of the Fourier image of the quantum confinement potential $U\left(k_z\right)$ for large k_z.

At the end of the overview of the theoretical model, we will dwell on one more question. One of the important features of polar InGaN/GaN quantum wells, which strongly affects the energy levels and the spatial distribution of wave functions, is the presence of polarization. The value of spontaneous polarization in quantum wells is defined by the difference between the constants of spontaneous polarization of the materials of the well itself and the barriers.

Since the polarization constants in binary GaN and InN are very close, this enables to assume that the spontaneous polarization in InGaN/GaN quantum wells will be much lower than the piezoelectric one [31]. Therefore, in this work, by polarization we understood its piezoelectric component. In the InGaN/GaN structures, the piezoelectric response to the appearence of tensile deformation in the direction of the polar axis (which coincides with the z-direction in our case) can be taken into account by using the well-known relation [32]:

$$P_z = 2\varepsilon_{xx}\left(e_{31} - e_{33}\frac{C_{13}}{C_{33}}\right), \tag{5}$$

where P_z is the component of the piezoelectric polarization vector in the z-direction, e_{31}, e_{33} – components of the piezoelectric tensor, C_{13}, C_{33} – components of the elasticity tensor, ε_{xx} – relative strain in the well plane, which is usually calculated from the difference between the crystal lattice parameters for GaN and InGaN $\varepsilon_{xx} = \left|a_{\mathrm{GaN}} - a_{\mathrm{InGaN}}\right| / a_{\mathrm{InGaN}}$. The crystal lattice parameters, elastic and piezoelectric constants for $\mathrm{In_xGa_{1-x}N}$ were found by linear interpolation between the values for GaN and InN listed in Table 2.

Since the value of the relative deformation ε_{xx} is negative for the well and positive for the barrier, the piezoelectric polarization vectors have opposite directions in the well and barriers. The potential of polarization field was obtained from

Table 2. Crystal lattice parameters, elastic and piezoelectric constants for binary nitrides.

	GaN	InN
a (Å)	3.189 [33]	3.544 [33]
c (Å)	5.185 [33]	5.718 [33]
C_{13} (GPa)	106 [34]	108 [35]
C_{33} (GPa)	398 [34]	265 [35]
e_{31} (C/m^2)	–0.44 [33]	–0.59 [33]
e_{33}(C/m^2)	0.75 [33]	1.14 [33]

$$U_P(z) = \begin{cases} \dfrac{P_{z,w}}{2\varepsilon_w\varepsilon_0}\left(z - \left(z_{0,w} - d_w/2\right)\right), & z \in QW \\ \dfrac{P_{z,b}}{2\varepsilon_b\varepsilon_0}\left(z - \left(z_{0,b} - d_b/2\right)\right), & z \in BR \end{cases} \tag{6}$$

where $\varepsilon_{w(b)}$, $d_{w(b)}$ and $z_{0,w(b)}$ are the dielectric function, thickness, and coordinate of the center of the well (w) and the barrier (b), respectively. To take into account polarization effects, the potential (3), or rather its Fourier image, must be added to the quantum confinement potential in (1).

Calculation of the Fourier image of polarization potential is actually the final stage in formation of the Hamiltonian matrix (4), after which we proceeded to its diagonalization. Diagonalization was carried out in the standard sequence: reducing the complex Hermitian matrix to a real tridiagonal matrix by means of unitary transformations; finding the eigenvalues of a tridiagonal matrix by using the bisection method; finding the eigenfunctions of the Hermitian matrix by using the inverse iteration method.

3. Results and discussion

The model described above was applied both to a single quantum well and to a system of five consecutive InGaN/GaN quantum wells. The five-well system is of particular practical interest for optoelectronics, since just this configuration of the active region is used in the vast majority of LEDs in the visible spectral region.

To evaluate the effectiveness of the developed model, we used the simplest rectangular shape of a quantum well surrounded by two barriers (Fig. 1b). The parameters of this structure are the depth and thickness of the well and the thickness of the barriers. The depth of the well was defined by the content of indium x in the ternary compound $\mathrm{In_xGa_{1-x}N}$ and the ratio of band gaps at the boundary of the well and barrier. All calculations in this work were performed for $x = 0.3$ and the ratio of band gaps $\Delta E_c / \Delta E_v = 70:30$ [36]. Under these conditions, the well depth for electrons is 0.75 eV, and that for holes is 0.32 eV. The thickness of one well was assumed to be equal to four constants of the crystal lattice in the polar direction $d_w = 4c$, which is approximately 2.0 nm (insignificant deviations related with the dependence of c on the content of In in the InGaN well).

The thickness of the barriers was the same $d_{br} = d_w$. Since the periodic boundary conditions were used in the derivation of the Hamiltonian matrix (4), the length of the considered nanostructure L_z (which is also the length of the periodicity) should be larger as compared to the thickness of the well with barriers in order to minimize the influence of boundary effects. When moving from direct to inverse space, the length L_z will be related to the discretization interval Δk_z by the ratio $L_z = 2\pi/\Delta k_z$.

According to our choice of eigenstate vectors $\Delta k_z = \pi/\left(N_{k_z} c\right)$, therefore $L_z = 2N_{k_z} c$. The latter relation sets a lower boundary for the discretization numbers N_{k_z}. If the total thickness of the well and barriers $d_w + 2d_{br} = 12c$, then the length of the periodicity should be at least twice as long, *i.e.* $L_z \approx 24c$. This means that N_{k_z} cannot be less than 12, and in the case of five consecutive wells $N_{k_z} > 44$. This is quite important, because N_{k_z} defines the dimensionality of the Hamiltonian matrix (4), and therefore will affect the rate of its numerical diagonalization.

The use of small discretization numbers that provide fast convergence of numerical diagonalization algorithms can lead to unreliable and sometimes controversial results. Also, the discretization numbers given above are only theoretical limits. More accurate values should be obtained using test calculations. The results of these tests for the ground state of the conduction band are shown in Fig. 2. It can be seen from them that $N_{k_z} = 31$ can be considered the most reasonable choice from the viewpoint of calculation error and calculation time. For a structure containing five wells separated by four barriers, the most optimal choice will be $N_{k_z} \approx 93$. All subsequent results were obtained with these discretization numbers. It should be noted that the calculation time of one quantum state in an isolated well on a dual-core Intel Core i3 (2.10 GHz) processor is approximately 4 s (for five wells, it is close to 38 s).

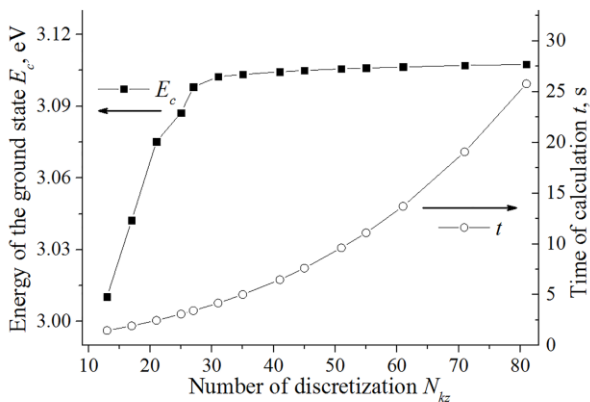

Fig. 2. Dependence of the energy of ground state for electrons in a quantum well and the time of calculation of this state on the number of discretization N_{k_z}.

This is quite close to the results typical of the simplified model of envelope functions. For states in the valence band, the time is several times longer. It is caused by the different number of bulk bands N_n, the overlap between which was taken into account for modeling the quantum states in the conduction band and valence one. For the states of conduction band, it was sufficient to include only two lowest bulk bands ($N_n = 2$). However, the complex structure of closely spaced valence bands of bulk nitrides requires the inclusion of a larger number of them in the calculation. The performed evaluations showed that it is optimal to include the five highest bulk bands ($N_n = 5$). As a result, for one isolated quantum well, the basis set contained 126 Bloch functions for modeling the electronic states and 315 Bloch functions for hole states.

Fig. 3 shows the energy band diagram of an isolated InGaN/GaN well along characteristic lines in the 2D Brillouin zone. Since the described algorithm for building a basic set of functions for the ground state ($\vec{k} = 0$) absolutely does not differ from the algorithm for an arbitrary other state ($\vec{k} \neq 0$) related to the 2D Brillouin zone, the time required for diagonalization of the matrix (4) does not depend on $\vec{k}$. It enables to effectively use the

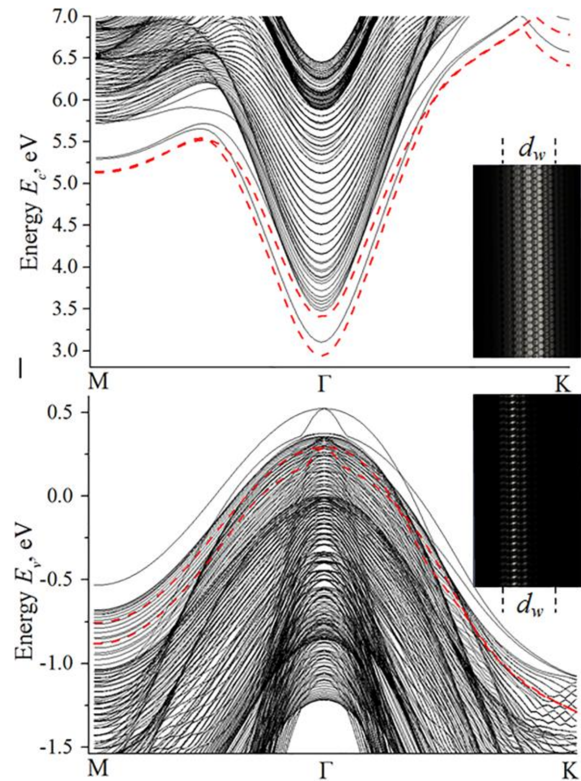

Fig. 3. Energy band diagram of an isolated InGaN/GaN quantum well along the characteristic M-G-K lines (shown in Fig. 1) in the 2D Brillouin zone. The red dashed lines show the positions of the first two energy bands in the absence of polarization in the well and barriers. The insets show the spatial distributions for the square of modulus corresponding to the wave functions for the ground state of electrons and holes in the plane along the direction of quantization.

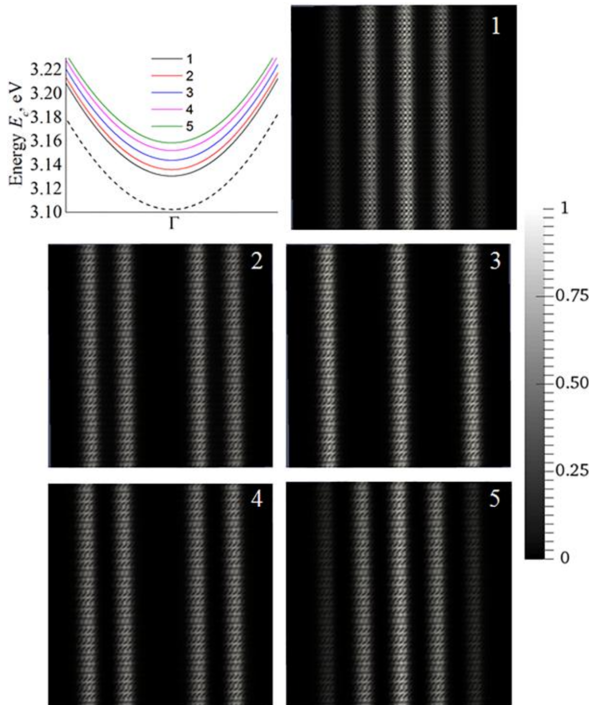

Fig. 4. Comparison of band diagrams in the vicinity of the ground state (Γ) of electrons for an isolated quantum well (dashed curve) and a structure of five consecutive InGaN/GaN wells. Indices 1–5 number the split energy levels in the five-well structure and the spatial distributions of the wave functions at the Γ point at each of the split levels in the plane along the quantization direction.

proposed LCBB approach in those practical problems, where it is necessary to know the band diagram for a large number of wave vectors $\vec{k}$ lying throughout the 2D Brillouin zone, and not only in the vicinity of $\vec{k} = 0$. In order to assess the influence of polarization effects on the shift of energy bands, the positions of the first two quantization bands in wells without taking polarization into account are indicated by dashed red lines in Fig. 3.

The influence of polarization can be also clearly seen in the spatial distributions of the square of the modulus of the wave function for the ground state in the plane along the direction of quantization, which is shown in the insets of Fig. 3. These distributions once again confirm effect of reducing the overlap of wave functions for electrons and holes under the influence of polarization field, which is well-known in polar InGaN/GaN quantum wells. But, unlike calculations in the effective mass approximation, the LCBB formalism also takes into account the atomistic nature of the wave function, as a result of which the spatial distribution does not have a typical smooth shape with one maximum shifted from the center, but contains local oscillations related with the placement of atoms.

Calculation for a sequence of five quantum wells revealed several interesting features. First, each quantum state in one isolated well splits into five states very close in energy (Fig. 4). For example, for the ground electronic state, the splitting is close to 0.03 eV. This effect also has the same origin as formation of minibands in the classical Kronig–Penny model for a particle in a periodic potential. Secondly, the spatial distributions of the wave functions of the split states are quite different from each other (Fig. 4). This result shows that one should distinguish between the wave functions in a system of coupled (and even weakly coupled) quantum wells and wave functions of quasi-isolated wells "stitched" with boundary conditions. The different overlap of the wave functions of electrons and holes will primarily be reflected on the optical and Coulomb matrix elements, and this directly affects the rates of radiative and non-radiative recombination.

Therefore, the currently known numerical estimates of the recombination coefficients and, in general, the mechanisms of the origin of non-trivial effects in InGaN/GaN LEDs, which were obtained for the model of one isolated well, should be revised with account of the above-mentioned splitting.

4. Conclusions

In this work, it has been shown that the formalism of the linear combination of bulk bands together with the effective pseudopotential method can be successfully used to calculate electronic states in 2D quantum structures based on $A^{III}B^{V}$ nitrides. In contrast to previous publications, we have presented the formalism of LCBB for materials with a wurtzite-type crystal lattice, *i.e.*, with a non-cubic lattice symmetry.

An algorithm for building the system of basis functions for representing the quantum state at an arbitrary $\vec{k}$ point of the 2D Brillouin zone has been proposed. Parameters and implementation of the developed approach has been realized for isolated polar InGaN/GaN quantum wells and their related systems. In both cases, the calculated efficiency of the approach closed in the traditional methods of envelope functions in the approximation of effective mass.

This opens possibilities for use in transport and recombination problems, where it is necessary to know the band diagram actually over the entire 2D Brillouin zone, and not just near the ground state, as is the case in the method of envelope functions. In this work, we limited ourselves to systems of rectangular quantum wells, although applying the method to more complex systems does not cause difficulties. In addition, combining the LCBB formalism with the diffusion-drift approach to build a self-consistent model of InGaN/GaN quantum wells without an empirical form of the quantum-dimensional potential looks potentially interesting.

References

1. Even A., Laval G., Ledoux O. *et al*. Enhanced In incorporation in full InGaN heterostructure grown on relaxed InGaN pseudo-substrate. *Appl. Phys. Lett.* 2017. **110**. P. 262103. https://doi.org/10.1063/1.4989998.

2. Zhuang Zh., Iida D., Ohkawa K. InGaN-based red light-emitting diodes: from traditional to micro-LEDs. *Jpn. J. Appl. Phys.* 2022. **61**. P. SA0809. https://doi.org/10.35848/1347-4065/ac1a00.
3. Ding K., Avrutin V., Izyumskaya N. *et al.* Micro-LEDs, a manufacturability perspective. *Appl. Sci.* 2019. **9**. P. 1206. https://doi.org/10.3390/app9061206.
4. Wong M.S., Nakamura S., DenBaars S.P. Review – progress in high performance III-nitride micro-light-emitting diodes. *ECS J. Solid State Sci. Technol.* 2019. **9**. P. 015012. https://doi.org/10.1149/2.0302001JSS.
5. Wong M.S., Kearns J.A., Lee C. *et al.* Improved performance of AlGaInP red micro-light-emitting diodes with sidewall treatments. *Opt. Exp.* 2020. **28**, Issue 4. P. 5787–5793. https://doi.org/10.1364/OE.384127.
6. Zhuang Z., Iida D., Ohkawa K. Effects of size on the electrical and optical properties of InGaN-based red light-emitting diodes. *Appl. Phys. Lett*. 2020. **116**. P. 173501. https://doi.org/10.1063/5.0006910.
7. Li P., David A., Li H. *et al.* High-temperature electroluminescence properties of InGaN red 40×40 μm^2 micro-light-emitting diodes with a peak external quantum efficiency of 3.2%. *Appl. Phys. Lett.* 2021. **119**. P. 231101. https://doi.org/10.1063/5.0070275.
8. Iida D., Niwa K., Kamiyama S., Ohkawa K. Demonstration of InGaN-based orange LEDs with hybrid multiple-quantum-wells structure. *Appl. Phys. Express.* 2016. **9**. P. 111003. https://doi.org/10.7567/APEX.9.111003.
9. Mitchell B., Dierolf V., Gregorkiewicz T., Fujiwara Y. Perspective: Toward efficient GaN-based red light emitting diodes using europium doping. *J. Appl. Phys.* 2018. **123**. P. 160901. https://doi.org/10.1063/1.5010762.
10. Jiang F., Zhang J., Xu L. *et al.* Efficient InGaN-based yellow-light-emitting diodes. *Photonics Research*. 2019. **7**, Issue 2. P. 144–148. https://doi.org/10.1364/PRJ.7.000144.11.
11. Ozaki T., Funato M., Kawakami Y. Red-emitting $In_xGa_{1-x}N/In_yGa_{1-y}N$ quantum wells grown on lattice-matched $In_yGa_{1-y}N/ScAlMgO_4$(0001) templates. *Appl. Phys. Express*. 2019. **12**. P. 011007. https://doi.org/10.7567/1882-0786/aaf4b1.
12. Huang Yu-M., Peng Ch.-Y., Miao W.-Ch. *et al.* High-efficiency InGaN red micro-LEDs for visible light communication. *Photonics Research.* 2022. **8**. P. 1978–1986. https://doi.org/10.1364/PRJ.462050.
13. Huang H.-H., Huang S.-K., Tsai Y.-L. *et al.* Investigation on reliability of red micro-light emitting diodes with atomic layer deposition passivation layers. *Opt. Exp.* 2020. **28**, Issue 25. P. 38184–38195. https://doi.org/10.1364/OE.411591.
14. Iida D., Zhuang Z., Kirilenko P. *et al.* Demonstration of low forward voltage InGaN-based red LEDs. *Appl. Phys. Express.* 2020. **13**. P. 031001. https://doi.org/10.35848/1882-0786/ab7168.
15. Ohkawa K., Zhuang Z., Iida D., Velazquez-Rizo M. InGaN-based RGB micro-LED arrays. *Proc. SPIE*. 2022. **PC12022**.
16. Iida D., Zhuang Zh., Kirilenko P. *et al.* 633-nm InGaN-based red LEDs grown on thick underlying GaN layers with reduced in-plane residual stress. *Appl. Phys. Lett.* 2020. **116**. P. 162101. https://doi.org/10.1063/1.5142538.
17. Ohkawa K., Ichinohe F., Watanabe T. *et al.* Metal-organic vapor-phase epitaxial growth simulation to realize high-quality and high-In-content InGaN alloys. *J. Cryst. Growth.* 2019. **512**. P. 69–73. https://doi.org/10.1016/j.jcrysgro.2019.02.018.
18. Burt M.G. The justification for applying the effective-mass approximation to microstructures. *J. Phys.: Condens. Matter.* 1992. **4**. P. 6651. https://doi.org/10.1088/0953-8984/4/32/003.
19. Pryor C. Eight-band calculations of strained InAs/GaAs quantum dots compared with one-, four-, and six-band approximations. *Phys. Rev. B.* 1998. **57**. P. 7190. https://doi.org/10.1103/PhysRevB.57.7190.
20. Jiang H., Singh J. Strain distribution and electronic spectra of InAs/GaAs self-assembled dots: An eight-band study. *Phys. Rev. B*. 1997. **56**. P. 4696. https://doi.org/10.1103/PhysRevB.56.4696.
21. Auf der Maur M. Multiscale approaches for the simulation of InGaN/GaN LEDs. *J. Comput. Electron*. 2015. **14**. P. 398–408. https://doi.org/10.1007/s10825-015-0683-3.
22. Lopez M., Sacconi F., Auf der Maur M. *et al.* Atomistic simulation of InGaN/GaN quantum disk LEDs. *Opt. Quant. Electron.* 2012. **44**. P. 89–94. https://doi.org/10.1007/s11082-012-9554-3.
23. Auf der Maur M., Pecchia A., Penazzi G. *et al.* Efficiency drop in green InGaN/GaN light emitting diodes: The role of random alloy fluctuations. *Phys. Rev. Lett.* 2016. **116**. P. 027401. https://doi.org/10.1103/PhysRevLett.116.027401.
24. Tanner D.P., Caro M.A., O'Reilly E.P., Schulz S. Atomistic analysis of the electronic structure of m-plane InGaN/GaN quantum wells: Carrier localization effects in ground and excited states due to random alloy fluctuations. *phys. status solidi (b).* 2016. **253**, Issue 5. P. 853–860. https://doi.org/10.1002/pssb.201552642.
25. Wang L.W., Franceschetti A., Zunger A. Million-atom pseudopotential calculation of G-X mixing in $GaAs_yAlAs$ superlattices and quantum dots. *Phys. Rev. Lett.* 1997. **78**, No 14. P. 2819–2822. https://doi.org/10.1103/PhysRevLett.78.2819.
26. Wang L.W., Zunger A. Linear combination of bulk bands method for large-scale electronic structure calculations on strained nanostructures. *Phys. Rev. B*. 1999. **59**. P. 15806. https://doi.org/10.1103/PhysRevB.59.15806.
27. Esseni D., Palestri P. Linear combination of bulk bands method for investigating the low-dimensional electron gas in nanostructured devices. *Phys. Rev. B*. 2005. **72**. P. 165342. https://doi.org/10.1103/PhysRevB.72.165342.

28. Pala M.G., Esseni D. Full-band quantum simulation of electron devices with the pseudopotential method: Theory, implementation, and applications. *Phys. Rev. B.* 2018. **97**. P. 125310. https://doi.org/10.1103/PhysRevB.97.125310.
29. Gill Ph.E., Murray W., Wright M.H. *Practical Optimization*. Academic Press, London, 2019. https://doi.org/10.1137/1.9781611975604.
30. Shchepetilnikov A.V., Khisameeva A.R., Solovyev V.V. *et al*. Spin-orbit interaction in GaN/AlGaN heterojunctions probed by electron spin resonance. *Phys. Rev. Appl.* 2022. **18**. P. 024037. https://doi.org/10.1103/PhysRevApplied.18.024037.
31. Bernardini F., Fiorentini V. Spontaneous versus piezoelectric polarization in III-V nitrides: Conceptual aspects and practical consequences. *phys. status solidi (b).* 1999. **216**, No 1. P. 391–398. https://doi.org/10.1002/(SICI)1521-3951(199911)216:1<391::AID-PSSB391>3.0.CO;2-K.
32. Wei Q.Y., Li T., Wu Z.H., Ponce F.A. In-plane polarization of GaN-based heterostructures with arbitrary crystal orientation. *phys. status solidi (b).* 2010. **207**, No 10. P. 2226–2232. https://doi.org/10.1002/pssa.200925632.
33. Prodhomme P.Y., Beya-Wakata A., Bester G. Nonlinear piezoelectricity in wurtzite semiconductors. *Phys. Rev. B.* 2013. **88**. P. 121304(R). https://doi.org/10.1103/PhysRevB.88.121304.
34. Soumelidou M.M., Belabbas I., Kioseoglou J. *et al*. Strain and elastic constants of GaN and InN. *Comput. Condens. Matter.* 2017. **10**. P. 25–30. https://doi.org/10.1016/j.cocom.2017.02.001.
35. Hattabi I., Abdiche A., Naqib S.H., Khenata R. First-principles calculations of elastic and thermodynamic properties under hydrostatic pressure of cubic InN_xP_{1-x} ternary alloys. *Chin. J. Phys.* 2019. **59**. P. 449–464. https://doi.org/10.1016/j.cjph.2019.04.011.
36. Mahmood Z.H., Shah A.P., Kadir A. *et al*. Determination of InN–GaN heterostructure band offsets from internal photoemission measurements. *Appl. Phys. Lett.* 2007. **91**. P. 152108. https://doi.org/10.1063/1.2794788.

Authors and CV

Slipokurov V.A. PhD in Technical Sciences, Researcher at the V. Lashkaryov Institute of Semiconductor Physics, NAS of Ukraine. Authored more than 30 publications. The area of his scientific interests is semiconductor physics and contact phenomena in semiconductors.
https://orcid.org/0009-0005-8095-8183

Korniychuk P.P. PhD in Liquid Crystal Physics, Associate Professor of the Department of Physics, Zhytomyr Ivan Franko State University. Authored more than 30 publications. The area of his scientific interests is organic semiconductor physics.
E-mail: korniypp@gmail.com,
https://orcid.org/0000-0002-1055-2007

Zinovchuk A.V. PhD in Solid-State Physics, Head of the Department of Physics at the Zhytomyr Ivan Franko State University. Authored more than 30 publications. The area of of scientific interests is semiconductor physics and physics of low-dimensional structures. https://orcid.org/0000-0003-1376-853X

Authors' contributions

Slipokurov V.A.: conceptualization, formal analysis, validation, writing – review & editing, project administration.

Korniychuk P.P: theoretical investigations, editing, literary research.

Zinovchuk A.V.: conceptualization, formal analysis, theoretical investigations, writing – original draft, editing.

All authors discussed the results and commented on the manuscript.

Метод швидкого розрахунку електронних станів у 2D квантових структурах на основі нітридів $A^{III}B^{V}$

А.В. Сліпокуров, П.П. Корнійчук, А.В. Зіновчук

Анотація. У роботі наведено метод швидкого розрахунку електронних станів у двовимірних квантових структурах на основі нітридів $A^{III}B^{V}$. Метод базується на представленні електронних станів у вигляді лінійної комбінації об’ємних хвильових функцій матеріалів, з яких виготовлені квантові структури. Розглянуто параметри та критерії відбору об’ємних хвильових функцій, які забезпечують швидку збіжність чисельних процедур розрахунку власних значень квантового гамільтоніану. Наведено результати розрахунків як для однієї полярної InGaN/GaN квантової ями, так і для системи з декількох квантових ям. Базуючись на повній зонній структурі $A^{III}B^{V}$ нітридів з кристалічною ґраткою типу вюртциту, пропонований підхід враховує стани, далекі від центра зони Бриллюена, водночас зберігаючи розрахункову ефективність традиційних методів огинаючих функцій у наближенні ефективної маси.

Ключові слова: $A^{III}B^{V}$ нітриди, двовимірні квантові структури, електронні стани.